

Magnetotransport in the double-atomic-layer $\text{rect-}\sqrt{7} \times \sqrt{3}\text{-In}$ phase on Si(111)

N. V. Denisov ¹, A. V. Matetskii ^{1,2}, A. N. Mihalyuk ^{1,3}, D. V. Gruznev ¹, A. V. Zotov ¹ and A. A. Saranin ¹

¹*Institute of Automation and Control Processes, FEB RAS, Vladivostok 690041, Russia*

²*Istituto di Struttura della Materia, Consiglio Nazionale delle Ricerche, I-34149 Trieste, Italy*

³*Institute of High Technologies and Advanced Materials, Far Eastern Federal University, Vladivostok 690950, Russia*



(Received 9 January 2023; accepted 5 May 2023; published 25 May 2023)

Magnetoresistance of the double-atomic-layer $\text{rect-}\sqrt{7} \times \sqrt{3}\text{-In/Si(111)}$ phase was measured *in situ* using the four-point-probe technique in the temperature range from 2.5 to 33 K and magnetic fields from -8 to $+8$ T. The $\text{rect-}\sqrt{7} \times \sqrt{3}\text{-In/Si(111)}$ was found to demonstrate a classical quadratic behavior of magnetoresistance at fields lower than ~ 0.2 T, and a large positive linear magnetoresistance at fields up to 8 T in the low-temperature range of up to ~ 10 K. In contrast, the results obtained on the parent single- and double-atomic In layers formed on the $\text{NiSi}_2/\text{Si(111)}$ substrate show much lower values of magnetoresistance. In view of the density functional theory calculation results, which reveal the presence of tiny Fermi pockets in the $\text{rect-}\sqrt{7} \times \sqrt{3}\text{-In/Si(111)}$ electronic band structure, we attribute the observed large linear magnetoresistance at the low-temperature range to a quantum mechanical origin.

DOI: [10.1103/PhysRevB.107.195305](https://doi.org/10.1103/PhysRevB.107.195305)

I. INTRODUCTION

Metal films having a thickness of one or a few atomic layers grown on crystalline semiconductor substrates attract the considerable interest of researchers due to an abundance of structural and electronic properties. Indium-induced superstructures on Si(111) and, in particular, the so-called Si(111)- $\text{rect-}\sqrt{7} \times \sqrt{3}\text{-In}$ reconstruction are of special interest due to the emergence of superconductivity at the atomic-scale limit. The $\text{rect-}\sqrt{7} \times \sqrt{3}\text{-In}$ reconstruction was termed to indicate its quasirectangular appearance in scanning tunneling microscopy (STM) images, as well as to distinguish it from the $\text{hex-}\sqrt{7} \times \sqrt{3}\text{-In}$ reconstruction having a lower In coverage and quasihexagonal STM appearance [1]. Si(111)- $\text{rect-}\sqrt{7} \times \sqrt{3}\text{-In}$ has been established to incorporate 2.4 monolayers (ML) of In, where $1.0 \text{ ML} = 7.8 \times 10^{14} \text{ cm}^{-2}$, and has a double-atomic-layer structure [2,3]. The $\text{rect-}\sqrt{7} \times \sqrt{3}\text{-In}$ is metallic and converts into a superconductor state [4–10] at a critical temperature which in the optimized samples was close to that for the bulk In (i.e., 3.2 vs 3.4 K). Therefore, Si(111)- $\text{rect-}\sqrt{7} \times \sqrt{3}\text{-In}$ has been widely used as a prototype system to explore various aspects of superconductivity at the atomic-scale limit, including the role of disorder in the film [7,10], effects of the substrates [11–13] and molecular-adsorbate capping layers [14–16], as well as to assess the superconductivity-associated electron-phonon coupling effects [17,18]. Another item which attracts the interest of researchers to $\text{rect-}\sqrt{7} \times \sqrt{3}\text{-In}$ concerns the peculiarities of its electron band structure. The $\text{rect-}\sqrt{7} \times \sqrt{3}\text{-In}$ was recognized early on as a nearly-free-electron two-dimensional (2D) metal [19], but very recent investigations have revealed that it has a rather complicated electronic band structure, especially regarding its spin texture [8,20]. As concerns the effects of an applied magnetic field on the electronic transport in $\text{rect-}\sqrt{7} \times \sqrt{3}\text{-In}$, so far all of the available data regard the field-induced suppression of the superconductivity at temperatures below transition into the superconductor state.

The goal of the present study was to explore the magnetotransport properties of the $\text{rect-}\sqrt{7} \times \sqrt{3}\text{-In}$ normal-metal phase above the critical temperature and to associate the obtained results with the peculiarities of the system electron band structure. To visualize the scale of the observed effects, we have also conducted magnetotransport measurements on the parent systems, single-atom $1 \times 1\text{-In}$ and $2\sqrt{19} \times 2\sqrt{3}\text{-In}$ and double-atom $\text{rect-}\sqrt{7} \times \sqrt{3}\text{-In}$ layers grown on a Si(111) substrate capped with a single-layer NiSi_2 [13]. Seemingly more relevant single-atom $2 \times 2\text{-In}$ and $\text{hex-}\sqrt{7} \times \sqrt{3}$ phases grown on a bare Si(111) surface were excluded from the list, since they show up as insulators at low temperatures [21–26]. In contrast, the single-atom In layers grown in an $\text{In/NiSi}_2/\text{Si(111)}$ system, $1 \times 1\text{-In}$ and $2\sqrt{19} \times 2\sqrt{3}\text{-In}$, remain conductors at low temperatures. The $1 \times 1\text{-In}$ phase adopts 1.0 ML of In and has a structure similar to that of the T1 atomic layer on Si(111) [27]. The other single-atom In phase forming at ~ 1.5 ML of In also displays a 1×1 structure at room temperature (RT), but converts upon cooling to a striped structure having $2\sqrt{19} \times 2\sqrt{3}$ periodicity. The double-atomic-layer In film grown on $\text{NiSi}_2/\text{Si(111)}$ at ~ 2.5 ML of In appears to be structurally akin to the double-atomic-layer $\text{rect-}\sqrt{7} \times \sqrt{3}\text{-In}$ phase forming on a bare Si(111) substrate. It has been found that the $\text{rect-}\sqrt{7} \times \sqrt{3}\text{-In}$ on Si(111) stands apart from the other phases, as it demonstrates the greatest magnetoresistance with a linear dependence on the field down to the low-field values, that serves as an indication of the sensitive relationship between the structural, electronic, and transport properties of the metal atomic layers.

II. EXPERIMENTAL AND CALCULATION DETAILS

Sample preparation and transport measurements were conducted in the UNISOKU USM 1500 LT system, equipped with scanning tunneling microscopy (STM) and four-point-

probe (4PP) techniques, which provide measurements down to the lowest temperature of ~ 2 K with the ability to apply a magnetic field up to 8 T perpendicular to the sample surface with the help of a superconducting magnet. The probes used were gold wires of 0.1 mm in diameter equally spaced by 0.2 mm along a straight line. Atomically clean Si(111) 7×7 surfaces were prepared *in situ* by flashing to 1280 °C after the samples were first outgassed at 600 °C for several hours. In was deposited from a tantalum tube, and Ni from an electron beam evaporator.

To prepare the Si(111)-rect- $\sqrt{7} \times \sqrt{3}$ -In phase, a two-step procedure was used. In the first step, the Si(111) $\sqrt{3} \times \sqrt{3}$ -In surface with 1/3 ML of In was prepared using In deposition onto the Si(111) 7×7 surface held at ~ 500 °C. In the second step, In was deposited onto a $\sqrt{3} \times \sqrt{3}$ -In surface held at RT, until the rect- $\sqrt{7} \times \sqrt{3}$ -In phase covered the whole surface. In each step, the structure of the surface was controlled by STM. To form In/NiSi₂/Si(111) atomic sandwiches, we employed the procedures described in detail in Ref. [13]. In particular, in order to grow the 1×1 -In phase, a 2×2 -In film with 1.0 ML of In was grown first on a bare Si(111) surface, then 1.0 ML of Ni was deposited onto it at RT, followed by sample annealing at 300 °C, which results in Ni intercalation into the top Si(111) bilayer and the formation of single-layer NiSi₂ sandwiched between a Si(111) substrate and a capping In layer which adopts a 1×1 structure. The other In films on the NiSi₂/Si(111), $2\sqrt{19} \times 2\sqrt{3}$ -In and rect- $\sqrt{7} \times \sqrt{3}$ -In, were grown using RT deposition of In onto the Si(111)/NiSi₂/ 1×1 -In surface. The large-scale and close-up STM images of the surfaces under investigation are collected in Supplemental Material Fig. S1 [28].

The density functional theory (DFT) calculations were performed by using the Vienna *ab initio* simulation package (VASP) [29,30], with core electrons represented by projector augmented-wave (PAW) potentials [31,32]. To obtain an accurate Si band gap we applied the DFT-1/2 self-energy correction method [33]. A spin-orbit interaction (SOI) was included in all types of calculations. The Si(111) 1×1 -(In, Ni) cell geometry was simulated by a repeating slab of ten Si bilayers and a vacuum region of ~ 15 Å. Si atoms in the bottom three bilayers were fixed at their bulk positions, the top seven bilayers were allowed to fully relax, and dangling bonds on the bottom surface were saturated by hydrogen atoms. Γ -centered $12 \times 12 \times 1$ and $5 \times 7 \times 1$ *k*-point meshes were used to sample the 1×1 and $\sqrt{7} \times \sqrt{3}$ Brillouin zones, respectively. The geometry optimization was performed until the residual force was smaller than 10 meV/Å.

III. RESULTS AND DISCUSSION

To set the stage, let us recall that the classical electronic transport theory [34] shows that magnetoresistance (MR) in a conductor behaves as

$$\frac{\Delta\rho}{\rho_0} \propto \begin{cases} (\mu B)^2, & \mu B < 1, \\ C, & \mu B > 1, \end{cases} \quad (1)$$

where μ is the mobility, B is the magnetic field, $\Delta\rho = \rho_B - \rho_0$, ρ_0 is the resistance at zero field, and C is a constant. Thus, MR grows quadratically with the field and then reaches a saturation. A linear and nonsaturating dependence on B denotes a

TABLE I. Characteristics of the In/Si(111) and In/NiSi₂/Si(111) samples under investigation, including In coverage Θ , sheet resistance R_s at a temperature of 5 K, and the value of the $k_F l_0$.

Si(111)	NiSi ₂ /Si(111)	Θ (ML)	R_s (Ω/\square)	$k_F l_0$
rect- $\sqrt{7} \times \sqrt{3}^a$		2.4	41	630
	rect- $\sqrt{7} \times \sqrt{3}^b$	2.4	86	300
	$2\sqrt{19} \times 2\sqrt{3}^c$	~ 1.5	227	114
	1×1^c	1.0	861	30

^aDouble In layer.

^bDouble In layer on a single NiSi₂ layer.

^cSingle In layer on a single NiSi₂ layer.

departure from conventional behavior. Experimentally, linear MR (LMR) has been observed in a wide variety of 2D and 3D materials [35]. Notably, LMR has been found to arise from multiple factors ranging from classical [36–40] to quantum [41].

Bearing the above in mind, let us consider the results of the magnetotransport measurements presented in Fig. 1. In particular, Fig. 1(a) shows the temperature dependencies of the sheet resistance R_s for the rect- $\sqrt{7} \times \sqrt{3}$ -In phase grown on bare Si(111) (red curve) and In layers grown on Si(111) covered by a single-layer NiSi₂, rect- $\sqrt{7} \times \sqrt{3}$ -In (yellow curve), $2\sqrt{19} \times 2\sqrt{3}$ -In (green curve), and 1×1 -In (blue curve). Table I lists the main characteristics of the samples, including the values of $k_F l_0 = 2\pi\hbar/(e^2 R_s)$, where k_F is Fermi wavelength and l_0 is an elastic length, estimated using a simple 2D free-electron-gas model. As one can see, in all cases the $k_F l_0$ are much greater than unity, ensuring the Ioffe-Regel criterion for metallic conduction [42], hence all samples show up as good metals. Figure 1(b) shows magnetoresistance, defined as $[R_s(B) - R_s(0)]/R_s(0)$, for all samples acquired at a temperature of 5 K and a magnetic field ranging from -6 to $+6$ T. The magnetoresistance is positive for all samples and the largest for the rect- $\sqrt{7} \times \sqrt{3}$ grown on a bare Si(111) surface.

Figure 2 summarizes the data on the temperature dependencies of the magnetoresistance for all samples. Note that the upper limit for the temperatures under investigation was set at 33 K, because at higher temperatures the contribution from the conductance through the substrate becomes noticeable. One can see that in addition to the classical and quantum magnetoresistance there are two other contributions to the magnetoresistance at low fields and temperatures. The first one is associated with the weak antilocalization (WAL) effect [43], which comes from the quantum interference of the scattered electron waves. The magnetic field affects the interference amplitude and leads to positive MR for WAL. Specifically, MR versus field shows a dip in the low-field region for the case of WAL in the narrow-field region, typically of about 0.5 T. The quantum corrections are essential for the dirty-metal limit, when the elastic length l_0 is much less than the coherence length l_ϕ , $l_0 \ll l_\phi$, thus their contribution is especially apparent for the cases of the high-resistance 1×1 /NiSi₂/Si(111) and $2\sqrt{19} \times 2\sqrt{3}$ /NiSi₂/Si(111) samples. The second contribution is due to the magnetic-field

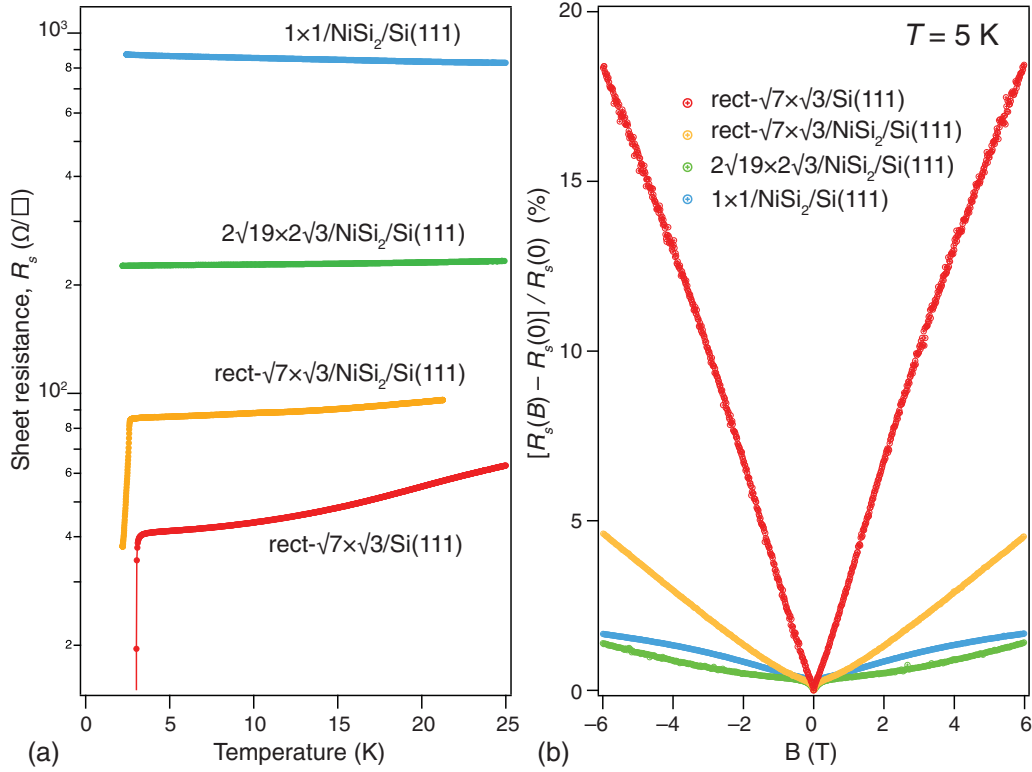


FIG. 1. (a) Temperature dependencies of the sheet resistance and (b) magnetoresistance at 5 K of the $\text{rect-}\sqrt{7} \times \sqrt{3}$ -In phase grown on the bare Si(111) (red curve) and In layers grown on the Si(111) covered by a single-layer NiSi_2 , $\text{rect-}\sqrt{7} \times \sqrt{3}$ -In (yellow curve), $2\sqrt{19} \times 2\sqrt{3}$ -In (green curve), and 1×1 -In (blue curve).

suppression of the superconductivity and superconductivity fluctuations. For the $\text{rect-}\sqrt{7} \times \sqrt{3}/\text{Si}(111)$ sample, it takes place in the vicinity of the superconducting transition temperature $\sim 2T_c \approx 6$ K and at magnetic fields lower than the upper critical field of 0.49 T at zero temperature [6]. Note that at 2.5 K the upper critical field is even lower, being about 0.1 T [6]. As one can see, these effects manifest themselves in the vertical shift of the MR data in Fig 2. Note that the low-temperature MR curves were shifted for the two superconducting double-layer-In samples shown in Figs. 2(a) and 2(b). In all cases, the low-field MR data were excluded from the data fit.

For fitting the results of measurements, the following formulas were found to be convenient to consider the case, when quadratic growth changes for the linear one [44],

$$\frac{\Delta R_s}{R_s(0)} = \beta \frac{B^2}{3B_k}, \quad B \leq B_k, \quad (2)$$

$$\frac{\Delta R_s}{R_s(0)} = \beta \left(B - B_k + \frac{B_k^2}{3B} \right), \quad B \geq B_k, \quad (3)$$

where $\Delta R_s(B) = R_s(B) - R_s(0)$, and β is a constant equal to the tangent of the angle between the asymptote and B axis. Note that the carrier mobility extracted from our MR data is $\mu_{\text{MR}}^2 = \beta/3B_k$.

As one can see in Figs. 2 and 3, the magnetoresistance $\Delta R_s(B)/R_s(0)$ is the largest for the $\text{rect-}\sqrt{7} \times \sqrt{3}/\text{Si}(111)$ sample, being 23% at 8 T. The sample demonstrates also the largest value of the slope of the LMR, as well the

largest value of the mobility μ_{MR} of $2700 \text{ cm}^2/(\text{V s})$ at low temperatures. In addition, the magnetoresistance of the $\text{rect-}\sqrt{7} \times \sqrt{3}/\text{Si}(111)$ is the only one which shows a strong temperature dependence.

The origin of the large LMR value for the $\text{rect-}\sqrt{7} \times \sqrt{3}/\text{Si}(111)$ sample, as compared to those for the other samples under investigation, is not completely clear. However, Abrikosov's theory of the quantum LMR [41] can be used in order to get a hint considering the sample electronic band structure. The presence of the two tiny Fermi pockets S'_4 and S'_5 , as evident from the spin-polarized DFT calculations around the \bar{Y} point of the surface Brillouin zone (SBZ) [see Fig. 4(d)] with an approximately linear crossing of the bands at the Fermi energy (within the numerical accuracy), is of particular essence here. The low density and small effective mass of the carriers due to the linear band crossing ensure that they can be confined to the lowest Landau level at low temperatures and thus reach the quantum limit. This leads to a LMR, given by [41]

$$\frac{\Delta R_s}{R_s(0)} = \frac{N_i B}{\pi n^2 e R_s(0)}, \quad (4)$$

where n is the density of electrons and N_i is the concentration of the static scattering centers. Such quantum MR is linear on B , positive, and nonsaturating.

Applicability of the theory of quantum LMR [41] requires $\hbar\omega_c \gg k_B T$, i.e., the temperature T should be small enough. Since the classic quadratic MR changes to LMR in our measurements on $\text{rect-}\sqrt{7} \times \sqrt{3}/\text{Si}(111)$ at $B \geq 0.2$ T

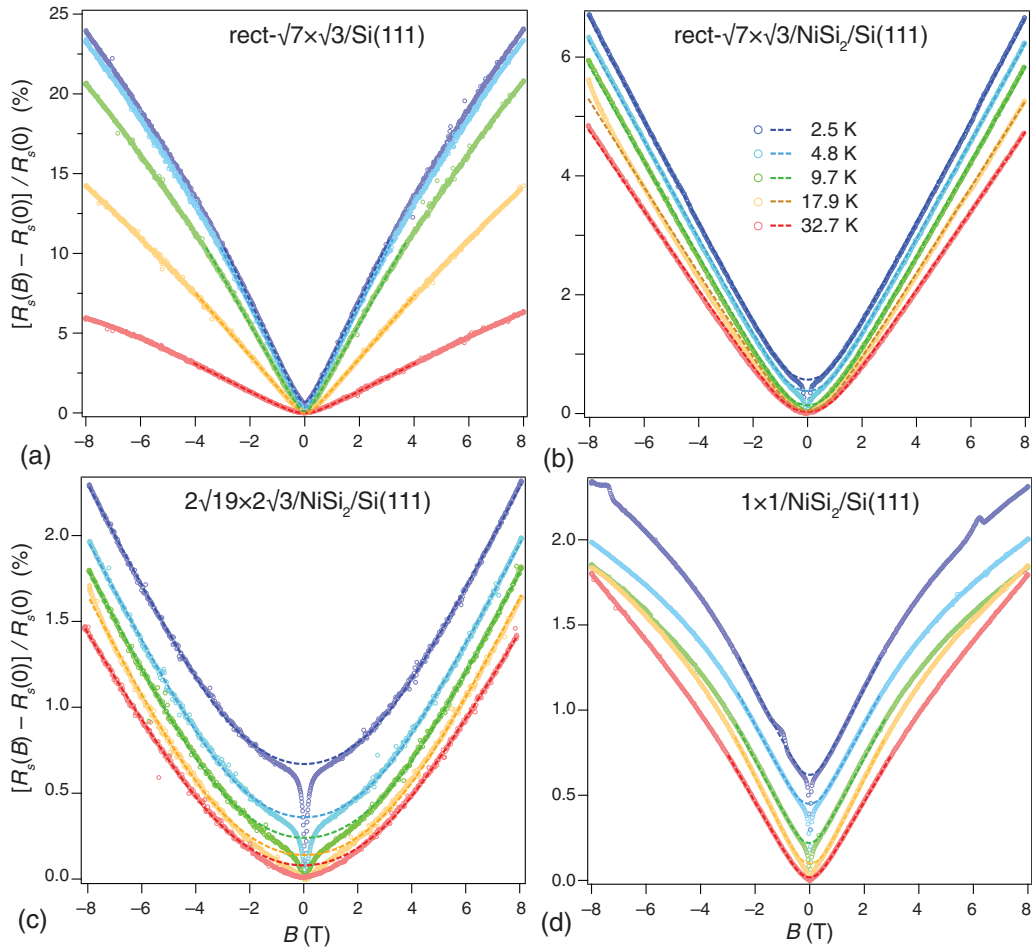


FIG. 2. Temperature dependencies of the magnetoresistance for (a) $\text{rect-}\sqrt{7} \times \sqrt{3}/\text{Si}(111)$, (b) $\text{rect-}\sqrt{7} \times \sqrt{3}/\text{NiSi}_2/\text{Si}(111)$, (c) $2\sqrt{19} \times 2\sqrt{3}/\text{NiSi}_2/\text{Si}(111)$, and (d) $1 \times 1/\text{NiSi}_2/\text{Si}(111)$ acquired at a magnetic field ranging from -8 to 8 T. Experimental data are represented by the circles, while the fit functions by the dashed lines. The close-up versions of the dependencies in the ± 3 T field range are presented in Supplemental Material Fig. S2 [28].

[see Fig. 3(c)], we take $B = 0.2$ T to calculate the upper temperature limit. A reasonable estimation for the effective mass of the carriers of the pockets according to the DFT calculations (see Table III) is $\sim 0.01\text{--}0.02m_0$ (m_0 is electronic rest mass). Substitution in the equation $\Delta E = \hbar\omega_c = \hbar eB/m^*$ gives a limit temperature of about $14\text{--}27$ K, which is reasonably consistent with our experimental observations, which show that the large LMR value and its independence of temperature persist for $\text{rect-}\sqrt{7} \times \sqrt{3}/\text{Si}(111)$ up to ~ 10 K.

TABLE II. Surface state (S_1 and S_2 holelike bands and S_3 electronlike band) band parameters of single-layer $1 \times 1/\text{NiSi}_2/\text{Si}(111)$, the absolute value of the effective mass m^* , the Fermi velocity v_F (10^8 cm/s), carrier concentration n (10^{14} cm^{-2}), elastic scattering time τ_e (fs), and carrier mobility μ [$\text{cm}^2/(\text{V s})$] evaluated from a comparison of the calculated band structure and transport measurements.

Band	m^*	v_F	n	τ_e	μ
S_1 (h)	1.71	1.11	0.61	28.1	28.9
S_2 (h)	2.17	0.88	0.99	35.4	28.8
S_3 (e)	2.37	0.81	0.92	38.4	-28.5

To tie together the electronic and transport properties, let us consider now the electronic band structure of $\text{rect-}\sqrt{7} \times \sqrt{3}/\text{Si}(111)$ in greater detail [Figs. 4(b) and 4(d)], in

TABLE III. Surface state (S_1 , S_2 , and S_3 electronlike bands and S_4 and S_5 holelike bands, tiny pockets S'_4 and S'_5 are electronlike and holelike, respectively) band parameters of double-layer $\text{rect-}\sqrt{7} \times \sqrt{3}/\text{Si}(111)$, the absolute value of the effective mass m^* , Fermi velocity v_F (10^8 cm/s), carrier concentration n (10^{14} cm^{-2}), elastic scattering time τ_e (fs), and carrier mobility μ [$\text{cm}^2/(\text{V s})$] evaluated from a comparison of the calculated band structure and transport measurements.

Band	m^*	v_F	n	τ_e	μ
S_1 (e)	1.58	0.97	0.182	222	-247
S_2 (e)	1.85	0.85	0.340	255	-242
S_3 (e)	1.16	1.16	1.370	161	-244
S_4 (h)	1.70	1.70	0.744	209	216
S'_4 (e)	~ 0.01	1.27	0.004	170	-42600
S_5 (h)	1.25	1.24	0.176	174	244
S'_5 (h)	~ 0.02	0.52	0.008	414	36400

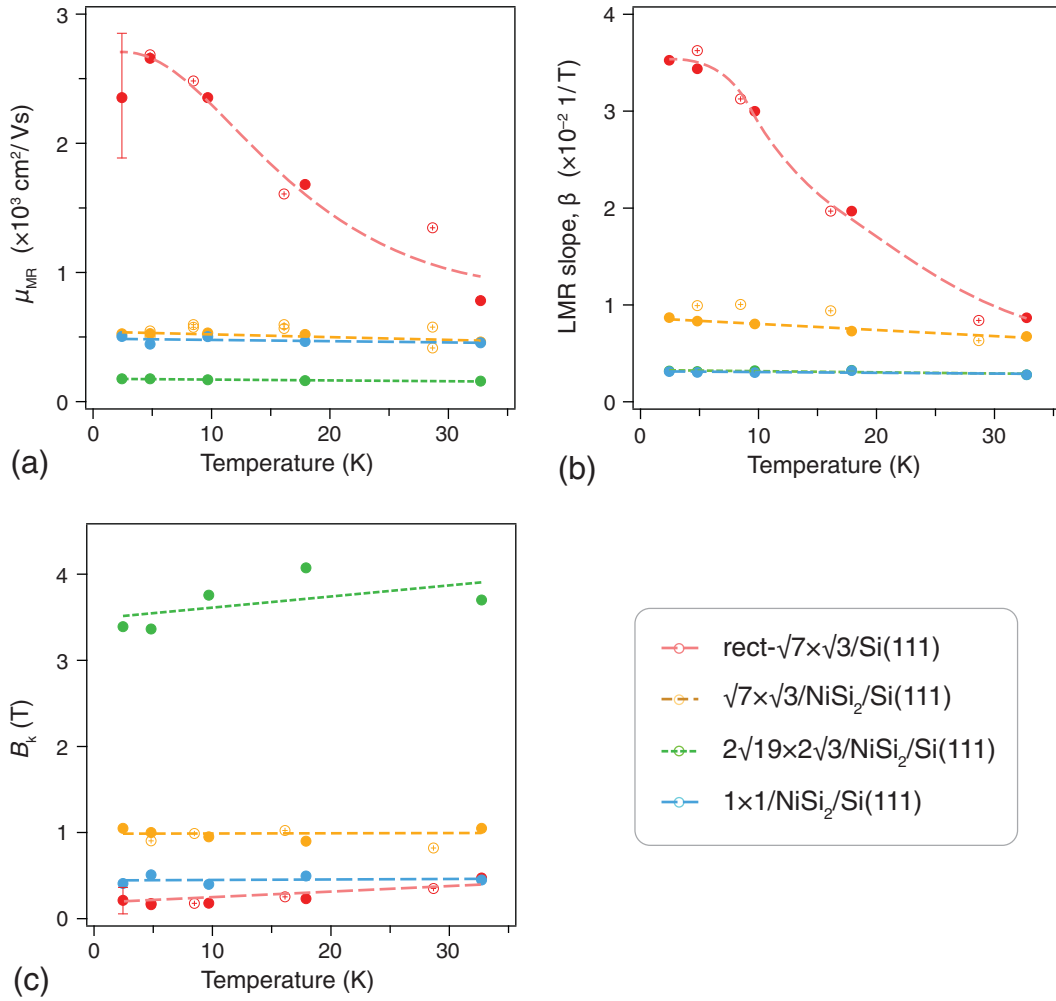


FIG. 3. Fitting parameters of Eqs. (2) and (3): (a) Mobility μ_{MR} , (b) LMR slope β , and (c) B_k extracted from the MR data shown in Fig. 2 for $\text{rect-}\sqrt{7} \times \sqrt{3}/\text{Si}(111)$, $\text{rect-}\sqrt{7} \times \sqrt{3}/\text{NiSi}_2/\text{Si}(111)$, $2\sqrt{19} \times 2\sqrt{3}/\text{NiSi}_2/\text{Si}(111)$, and $1 \times 1/\text{NiSi}_2/\text{Si}(111)$.

particular in comparison with that of $1 \times 1/\text{NiSi}_2/\text{Si}(111)$ [Figs. 4(a) and 4(c)]. The choice of $1 \times 1/\text{NiSi}_2/\text{Si}(111)$ among other $\text{In}/\text{NiSi}_2/\text{Si}(111)$ samples was dictated due to the insufficient knowledge of their electronic properties. In particular, the electronic band structure of $2\sqrt{19} \times 2\sqrt{3}/\text{NiSi}_2/\text{Si}(111)$ remains unknown due to the absence of an available model of its atomic structure [13]. Though the atomic structural model for $\sqrt{7} \times \sqrt{3}/\text{NiSi}_2/\text{Si}(111)$ was established, the absence of appropriate angle-resolved photoemission spectroscopy (ARPES) data excludes the possibility to determine the accurate position of the Fermi level, hence hampering meaningful discussions on the transport properties.

Let us start with a relatively more simple case of $1 \times 1/\text{NiSi}_2/\text{Si}(111)$. The results of previous investigations [13] showed that the position of the Fermi level deduced from the ARPES data of $1 \times 1/\text{NiSi}_2/\text{Si}(111)$ coincides with that found in the DFT calculations. One can see in Fig. 4(b) that the Fermi surface of $1 \times 1/\text{NiSi}_2/\text{Si}(111)$ has two hole pockets centered in the $\bar{\Gamma}$ points of the SBZ (denoted S_1 and S_2) with a negligible spin splitting and the one electron pocket centered in the \bar{K} point (denoted S_3) with a

small spin splitting. In order to estimate the conductivity of $1 \times 1/\text{NiSi}_2/\text{Si}(111)$, we extracted the carrier effective mass m^* and Fermi velocity v_F from the band-structure data (see Table II) and then estimated the conductivity as $\sigma = \sum_i \sigma_i = \sum_i q_i n_i \mu_i$, where n_i and μ_i are the carrier density and mobility for a given band, and q_i is the carrier charge. Recall that for electrons, $q = -e$ and $\mu < 0$; for holes, $q = e$ and $\mu > 0$. For the electronic transport in metals at low temperatures, mobility can be expressed by a simple formula [45] $\mu = e\tau_e/m^*$, where m^* is a carrier effective mass and τ_e is an elastic relaxation time, which is related to electron elastic length l_0 and Fermi velocity v_F as $l_0 = v_F\tau_e$ and is assumed to be the same for all bands, being determined solely by the density of the defects. For $R_s = 861 \Omega/\square$, this gives an elastic length $l_0 = 311 \text{ \AA}$. A positive value of the effective Hall mobility, $\mu_{\text{eff}} = +8.0 \text{ cm}^2/(\text{V s})$, indicates that $1 \times 1/\text{NiSi}_2/\text{Si}(111)$ is a hole metal, where $\mu_{\text{eff}} = \sum_i q_i n_i \mu_i^2 / \sum_i q_i n_i \mu_i$. It is worth noting that though the electronic band structure of $1 \times 1/\text{NiSi}_2/\text{Si}(111)$ does not contain appropriate pocket features, the sample displays LMR below 3 T, which can be attributed to the classical mechanism proposed by Parish and Littlewood [36].

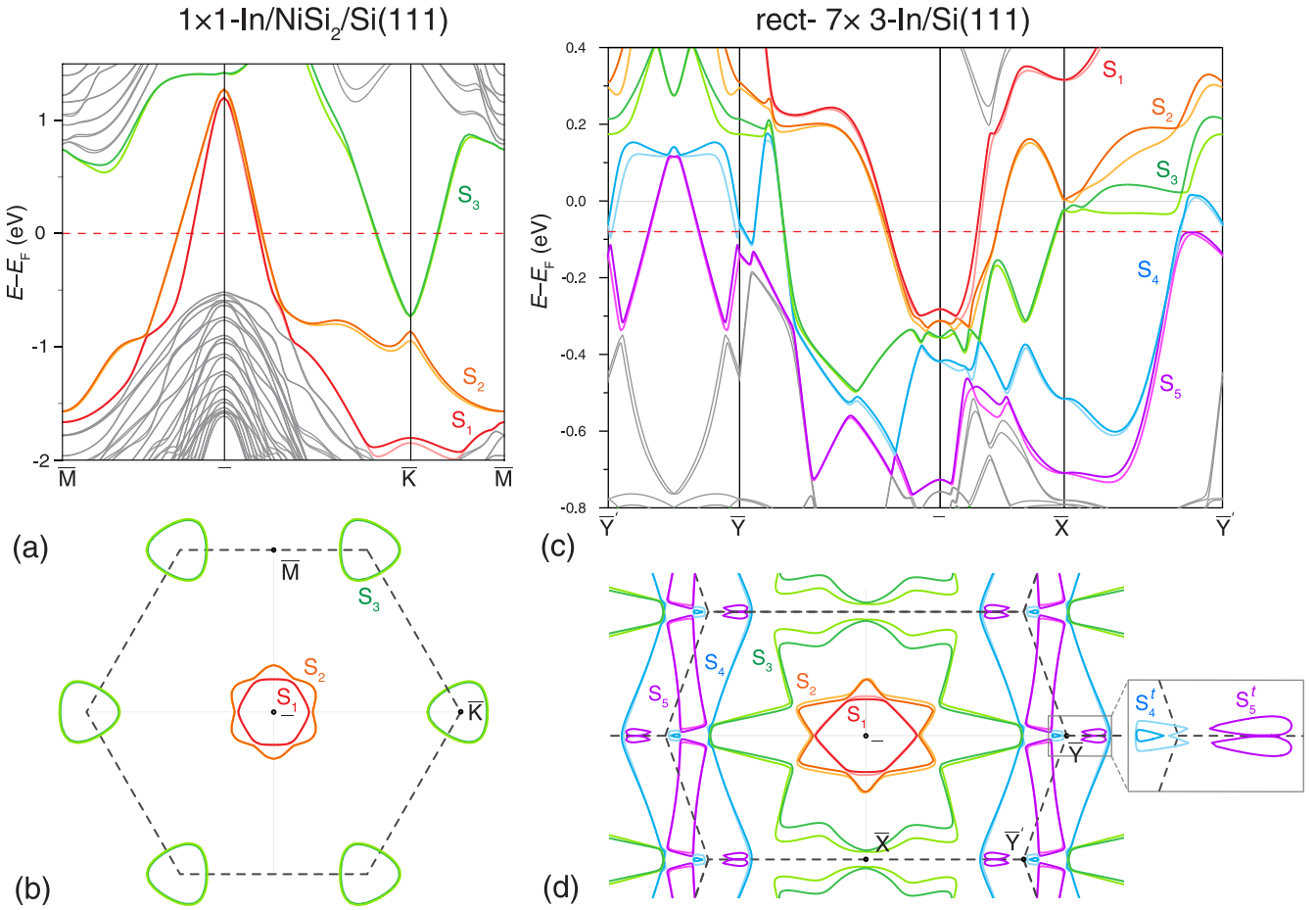


FIG. 4. (a), (c) Calculated electronic band structures and (b), (d) Fermi-surface maps of the In/NiSi₂/Si(111)1 × 1 and rect- $\sqrt{7} \times \sqrt{3}$ /Si(111) surfaces, respectively. To distinguish the bands, they are highlighted by different colors. The Fermi-level position is shown by the red dashed line. The inset in (d) shows the tiny pockets in the vicinity of the \bar{Y} point with a greater magnification.

For the rect- $\sqrt{7} \times \sqrt{3}$ /Si(111) sample, the position of the Fermi level was estimated through a comparison of the calculated constant-energy maps with the Fermi surface obtained with ARPES on the single-domain rect- $\sqrt{7} \times \sqrt{3}$ /Si(111) surfaces [8,19]. As a result of the evaluation, the calculated Fermi level was shifted by -80 meV. The corresponding band parameters for rect- $\sqrt{7} \times \sqrt{3}$ /Si(111) are listed in Table III. Using the same procedure as above for 1 × 1/NiSi₂/Si(111), we obtained that $R_s = 41 \Omega/\square$ for rect- $\sqrt{7} \times \sqrt{3}$ /Si(111) gives an elastic length $l_0 = 2966 \text{ \AA}$. A positive value of the effective Hall mobility $\mu_{\text{eff}} = +2907 \text{ cm}^2/(\text{V s})$ indicates that rect- $\sqrt{7} \times \sqrt{3}$ /Si(111) is also a hole metal. It is worth noting, however, that the value of the effective Hall mobility appears to be quite sensitive to the tiny Fermi pocket parameters. If one excludes them from the estimation, the effective Hall mobility changes sign and lowers the value by an order of magnitude to $\mu_{\text{eff}} = -236 \text{ cm}^2/(\text{V s})$. In this respect, the Hall measurements should be quite useful to evaluate the role of tiny Fermi pockets in the transport properties of rect- $\sqrt{7} \times \sqrt{3}$ /Si(111) samples.

IV. CONCLUSIONS

In conclusion, the magnetotransport properties of the double-atomic-layer rect- $\sqrt{7} \times \sqrt{3}$ -In phase grown on

Si(111), in comparison with those of the parent phases, double-atomic-layer rect- $\sqrt{7} \times \sqrt{3}$ -In and single-atomic-layer $2\sqrt{19} \times 2\sqrt{3}$ -In and 1×1 -In, grown on Si(111) terminated by a single-layer NiSi₂, were investigated at low temperatures ranging from 2.5 to 32.7 K and magnetic fields ranging from -8 to $+8$ T. It was found that among other phases the rect- $\sqrt{7} \times \sqrt{3}$ -In on Si(111) demonstrates the greatest magnetoresistance $[R_s(B) - R_s(0)]/R_s(0)$, which amounts to 23% at 2.5 K and 8 T. Magnetoresistance in rect- $\sqrt{7} \times \sqrt{3}$ /Si(111) shows a linear dependence on the field down to the low-field values, where it displays a temperature-dependent crossover to a classical quadratic behavior. The linear dependence on the field can be understood and described in the framework of Abrikosov's theory of quantum linear magnetoresistance [41]. We suggested that the transport properties and especially the value of the effective Hall mobility can be greatly affected by the tiny Fermi pockets present in the electronic band structure of the rect- $\sqrt{7} \times \sqrt{3}$ -In phase. The prospective Hall measurements are desirable to test this assumption, especially with a controlled changing of the Fermi-level position (e.g., using appropriate doping) to affect the feeling of those pockets. It was also found that the following phases, double-atomic-layer rect- $\sqrt{7} \times \sqrt{3}$ -In and single-atomic-layer $2\sqrt{19} \times 2\sqrt{3}$ -In and 1×1 -In, grown

on a NiSi₂/Si(111) substrate display much lower MR values. Bearing in mind that an added NiSi₂ layer affects both the structural and electronic properties of the In/Si(111) samples, it is difficult to distinguish which of the factors plays the most decisive role.

ACKNOWLEDGMENTS

The work was supported by the Russian Science Foundation (Grant No. 19-12-00101 [46]). The calculations were conducted using the equipment of Shared Resource Center “Far Eastern Computing Resource” IACP FEB RAS [47].

- [1] J. Kraft, M. G. Ramsey, and F. P. Netzer, Surface reconstructions of In on Si(111), *Phys. Rev. B* **55**, 5384 (1997).
- [2] J. W. Park and M. H. Kang, Double-layer in Structural Model for the In/Si(111)- $\sqrt{7} \times \sqrt{3}$ Surface, *Phys. Rev. Lett.* **109**, 166102 (2012).
- [3] T. Shirasawa, S. Yoshizawa, T. Takahashi, and T. Uchihashi, Structure determination of the Si(111)- $\sqrt{7} \times \sqrt{3}$ -In atomic-layer superconductor, *Phys. Rev. B* **99**, 100502(R) (2019).
- [4] T. Zhang, P. Cheng, W. J. Li, Y. J. Sun, G. Wang, X. G. Zhu, K. He, L. Wang, X. Ma, X. Chen, Y. Wang, Y. Liu, H. Q. Lin, J. F. Jia, and Q. K. Xue, Superconductivity in one-atomic-layer metal films grown on Si(111), *Nat. Phys.* **6**, 104 (2010).
- [5] T. Uchihashi, P. Mishra, M. Aono, and T. Nakayama, Macroscopic Superconducting Current Through a Silicon Surface Reconstruction with Indium Adatoms: Si(111)-($\sqrt{7} \times \sqrt{3}$)-In, *Phys. Rev. Lett.* **107**, 207001 (2011).
- [6] M. Yamada, T. Hirahara, and S. Hasegawa, Magnetoresistance Measurements of a Superconducting Surface State of In-Induced and Pb-Induced Structures on Si(111), *Phys. Rev. Lett.* **110**, 237001 (2013).
- [7] S. Yoshizawa, H. Kim, Y. Hasegawa, and T. Uchihashi, Disorder-induced suppression of superconductivity in the Si(111)-($\sqrt{7} \times \sqrt{3}$)-In surface: Scanning tunneling microscopy study, *Phys. Rev. B* **92**, 041410(R) (2015).
- [8] S. Yoshizawa, T. Kobayashi, Y. Nakata, K. Yaji, K. Yokota, F. Komori, S. Shin, K. Sakamoto, and T. Uchihashi, Atomic-layer Rashba-type superconductor protected by dynamic spin-momentum locking, *Nat. Commun.* **12**, 1462 (2021).
- [9] Y. Wu, M. C. Duan, N. Liu, G. Yao, D. Guan, S. Wang, Y. Y. Li, H. Zheng, C. Liu, and J. F. Jia, Diamagnetic response of a superconducting surface superstructure: Si(111)- $\sqrt{7} \times \sqrt{3}$ -In, *Phys. Rev. B* **99**, 140506(R) (2019).
- [10] Y. Wu, G. Yao, Y. Qu, X. Wang, N. Liu, M. C. Duan, D. D. Guan, S. Wang, H. Zheng, Y. Y. Li, C. Liu, and J. F. Jia, Influence of disorder on superconductivity in the Si(111)- $\sqrt{7} \times \sqrt{3}$ -In surface, *Appl. Phys. Lett.* **117**, 172601 (2020).
- [11] T. Ogino, I. Seo, H. Tajiri, M. Nakatake, S. I. Takakura, Y. Sato, Y. Hasegawa, Y. Gohda, K. Nakatsuji, and H. Hirayama, Superconductivity in a two monolayer thick indium film on Si(111)- $\sqrt{3} \times \sqrt{3}$ -B, *Phys. Rev. B* **106**, 045423 (2022).
- [12] S. Terakawa, S. Hatta, H. Okuyama, and T. Aruga, Ultrathin (In, Mg) films on Si(111): A nearly freestanding double-layer metal, *Phys. Rev. B* **105**, 125402 (2022).
- [13] L. V. Bondarenko, A. Y. Tupchaya, Y. E. Vekovshinin, D. V. Gruznev, A. N. Mihalyuk, N. V. Denisov, A. V. Matetskiy, A. V. Zotov, and A. A. Saranin, Single and double In atomic layers grown on top of a single atomic NiSi₂ layer on Si(111), *Phys. Rev. B* **106**, 035415 (2022).
- [14] S. Yoshizawa, E. Minamitani, S. Vijayaraghavan, P. Mishra, Y. Takagi, T. Yokoyama, H. Oba, J. Niita, W. Sakamoto, T. Nakayama, and T. Uchihashi, Controlled modification of superconductivity in epitaxial atomic layer-organic molecule heterostructures, *Nano Lett.* **17**, 2287 (2017).
- [15] R. Sagehashi, T. Kobayashi, T. Uchihashi, and K. Sakamoto, Tuning the Fermi surface of In/Si(111)-($\sqrt{7} \times \sqrt{3}$) by CuPc adsorption, *Surf. Sci.* **705**, 121777 (2021).
- [16] N. Sumi, Y. Yamada, M. Sasaki, R. Arafune, N. Takagi, S. Yoshizawa, and T. Uchihashi, Unsubstituted and fluorinated copper phthalocyanine overlayers on Si(111)-($\sqrt{7} \times \sqrt{3}$)-In surface: Adsorption geometry, charge polarization, and effects on superconductivity, *J. Phys. Chem. C* **123**, 8951 (2019).
- [17] S. H. Uhm and H. W. Yeom, Electron-phonon interaction of one-dimensional and two-dimensional surface states in indium adlayers on the Si(111) surface, *Phys. Rev. B* **86**, 245408 (2012).
- [18] I. Y. Sklyadneva, R. Heid, P. M. Echenique, and E. V. Chulkov, Electron-phonon interaction in In-induced $\sqrt{7} \times \sqrt{3}$ structures on Si(111) from first-principles, *Phys. Chem. Chem. Phys.* **23**, 7955 (2021).
- [19] E. Rotenberg, H. Koh, K. Rossnagel, H. W. Yeom, J. Schäfer, B. Krenzer, M. P. Rocha, and S. D. Kevan, Indium $\sqrt{7} \times \sqrt{3}$ on Si(111): A Nearly Free Electron Metal in Two Dimensions, *Phys. Rev. Lett.* **91**, 246404 (2003).
- [20] T. Kobayashi, Y. Nakata, K. Yaji, T. Shishidou, D. Agterberg, S. Yoshizawa, F. Komori, S. Shin, M. Weinert, T. Uchihashi, and K. Sakamoto, Orbital Angular Momentum Induced Spin Polarization of 2D Metallic Bands, *Phys. Rev. Lett.* **125**, 176401 (2020).
- [21] J. P. Chou, C. M. Wei, Y. L. Wang, D. V. Gruznev, L. V. Bondarenko, A. V. Matetskiy, A. Y. Tupchaya, A. V. Zotov, and A. A. Saranin, Atomic structure and electronic properties of the In/Si(111)₂ × 2 surface, *Phys. Rev. B* **89**, 155310 (2014).
- [22] S. G. Kwon and M. H. Kang, Honeycomb network of indium trimers and monomers on Si(111)-(2 × 2), *Phys. Rev. B* **89**, 165304 (2014).
- [23] J. W. Park and M. H. Kang, Single-Layer Limit of Metallic Indium Overlayers on Si(111), *Phys. Rev. Lett.* **117**, 116102 (2016).
- [24] S. Terakawa, S. Hatta, H. Okuyama, and T. Aruga, Structure and phase transition of a uniaxially incommensurate In monolayer on Si(111), *Phys. Rev. B* **100**, 115428 (2019).
- [25] A. A. Saranin, A. V. Zotov, M. Kishida, Y. Murata, S. Honda, M. Katayama, K. Oura, D. V. Gruznev, A. Visikovskiy, and H. Tochihara, Reversible phase transitions in the pseudomorphic $\sqrt{7} \times \sqrt{3}$ -hex In layer on Si(111), *Phys. Rev. B* **74**, 035436 (2006).
- [26] A. N. Mihalyuk, A. A. Alekseev, C. R. Hsing, C. M. Wei, D. V. Gruznev, L. V. Bondarenko, A. V. Matetskiy, A. Y. Tupchaya, A. V. Zotov, and A. A. Saranin, Low-temperature one-atom-layer $\sqrt{7} \times \sqrt{3}$ -In phase on Si(111), *Surf. Sci.* **649**, 14 (2016).
- [27] L. V. Bondarenko, A. Y. Tupchaya, A. N. Mihalyuk, S. V. Ereemeev, A. V. Matetskiy, N. V. Denisov, Y. E. Vekovshinin,

- A. V. Slyshkin, D. V. Gruznev, A. V. Zotov, and A. A. Saranin, Fabrication and characterization of a single monolayer NiSi₂ sandwiched between TI capping layer and a Si(111) substrate, *2D Mater.* **7**, 025009 (2020).
- [28] See Supplemental Material at <http://link.aps.org/supplemental/10.1103/PhysRevB.107.195305> for the large-scale and close-up STM images of the surfaces under investigation and the temperature dependencies of the magnetoresistance in the ± 3 T field range.
- [29] G. Kresse and J. Hafner, *Ab initio* molecular-dynamics simulation of the liquid-metal-amorphous-semiconductor transition in germanium, *Phys. Rev. B* **49**, 14251 (1994).
- [30] G. Kresse and J. Furthmüller, Efficiency of *ab-initio* total energy calculations for metals and semiconductors using a plane-wave basis set, *Comput. Mater. Sci.* **6**, 15 (1996).
- [31] P. E. Blöchl, Projector augmented-wave method, *Phys. Rev. B* **50**, 17953 (1994).
- [32] G. Kresse and D. Joubert, From ultrasoft pseudopotentials to the projector augmented-wave method, *Phys. Rev. B* **59**, 1758 (1999).
- [33] L. G. Ferreira, M. Marques, and L. K. Teles, Approximation to density functional theory for the calculation of band gaps of semiconductors, *Phys. Rev. B* **78**, 125116 (2008).
- [34] A. Abrikosov, *Fundamentals of the Theory of Metals* (North-Holland, Amsterdam, 1988), p. 630.
- [35] Q. Niu, W. C. Yu, K. Y. Yip, Z. L. Lim, H. Kotegawa, E. Matsuoka, H. Sugawara, H. Tou, Y. Yanase, and S. K. Goh, Quasilinear quantum magnetoresistance in pressure-induced nonsymmorphic superconductor chromium arsenide, *Nat. Commun.* **8**, 15358 (2017).
- [36] M. M. Parish and P. B. Littlewood, Non-saturating magnetoresistance in heavily disordered semiconductors, *Nature (London)* **426**, 162 (2003).
- [37] Y. Yan, L.-X. Wang, D.-P. Yu, and Z.-M. Liao, Large magnetoresistance in high mobility topological insulator Bi₂Se₃, *Appl. Phys. Lett.* **103**, 033106 (2013).
- [38] P. S. Alekseev, A. P. Dmitriev, I. V. Gornyi, V. Y. Kachorovskii, B. N. Narozhny, M. Schütt, and M. Titov, Magnetoresistance in Two-Component Systems, *Phys. Rev. Lett.* **114**, 156601 (2015).
- [39] J. C. W. Song, G. Refael, and P. A. Lee, Linear magnetoresistance in metals: Guiding center diffusion in a smooth random potential, *Phys. Rev. B* **92**, 180204 (2015).
- [40] T. Khouri, U. Zeitler, C. Reichl, W. Wegscheider, N. E. Hussey, S. Wiedmann, and J. C. Maan, Linear Magnetoresistance in a Quasifree Two-Dimensional Electron Gas in an Ultrahigh Mobility GaAs Quantum Well, *Phys. Rev. Lett.* **117**, 256601 (2016).
- [41] A. A. Abrikosov, Quantum magnetoresistance, *Phys. Rev. B* **58**, 2788 (1998).
- [42] A. F. Ioffe and A. R. Regel, Non-crystalline, amorphous, and liquid electronic semiconductors, in *Progress in Semiconductors*, edited by A. F. Gibson, F. A. Kroger, and R. E. Burgess (Heywood, London, 1960), Vol. 4, pp. 237–291.
- [43] G. Bergmann, Weak localization and its applications as an experimental tool, *Int. J. Mod. Phys. B* **24**, 2015 (2010).
- [44] P. Kapitza and E. Rutherford, The change of electrical conductivity in strong magnetic fields. Part I. Experimental results, *Proc. R. Soc. London, Ser. A* **123**, 292 (1929).
- [45] M. Myronov, Molecular beam epitaxy of high mobility silicon, silicon germanium and germanium quantum well heterostructures, in *Molecular Beam Epitaxy*, edited by M. Henini, 2nd ed. (Elsevier, Amsterdam, 2018), pp. 37–54.
- [46] <https://rscf.ru/project/19-12-00101/>.
- [47] <https://cc.dvo.ru>.